Advances in Nano Research, *Vol. 11, No. 1 (2021) 1-17*
https://doi.org/10.12989/anr.2021.11.1.001

Size-dependent vibration response of porous graded nanostructure with FEM and nonlocal continuum model

Yogesh Kumar[1], Ankit Gupta*[1] and Abdelouahed Tounsi[2,3]

[1]*School of Engineering, Shiv Nadar University, Gautama Buddha Nagar, India*
[2]*YFL (Yonsei Frontier Lab), Yonsei University, Seoul, Korea*
[3]*Department of Civil and Environmental Engineering, King Fahd University of Petroleum & Minerals, 31261 Dhahran, Eastern Province, Saudi Arabia*

(*Received April 30, 2020, Revised December 23, 2020, Accepted March 4, 2021*)

Abstract. In the present paper, a refined trigonometric higher-order shear deformation theory has been presented with the conjunction of nonlocal theory for the vibrational response of functionally graded (FG) porous nanoplate. The displacement field is chosen based on assumptions that the out of the plane displacement consists of bending and shear components whereas the transverse shear-strain has nonlinear variation along the thickness direction. The number of unknown variables is four, as against five in other renowned shear deformation theories. The governing equations have been derived using Hamilton's principle. A generalized porosity model has also been developed to accommodate both even and uneven type of distribution of porosity in the FG nanoplates. The closed-form solution of simply-supported FG porous nanoplates is obtained and the results are compared with the available reported results. In finite element solution, a C^0 continuous isoparametric quadrilateral element has been used with various conventional and unconventional boundary conditions. The effects of various parameters like small-scale effect, aspect ratio, volume fraction index, porosity volume fraction, and thickness ratio have been investigated. The significant influence of small-scale effects and porosity inclusions have been observed in the reported results. It has been reported that both closed-form and finite element solutions with the present theory can make accurate predictions of the free vibration response.

Keywords: closed-form solution; composite materials; functionally graded (FG) material; Hamilton's principle; Navier's solution; nonlocal theory; vibration analysis

1. Introduction

Functionally graded (FG) materials are a class of advanced composites in which the material properties gradually vary from one surface to another surface. Gradation in the material properties helps in reducing the stress concentrations, thermal and residual stresses and circumvent the shortcomings of conventional laminated composites (Gupta and Talha 2017, 2018a). Koizumi (1997) proposed the concept of FG material in 1984 intending to prepare thermal barrier materials. Several reports are available which dealt with the structural response of FG plates subjected to various loading, and boundary conditions. In the past two decades, the application of nanomaterials in micro-electro-mechanical systems (MEMS) and nano-electro-mechanical systems (NEMS) has significantly augmented due to their extraordinary mechanical, chemical, and electronic properties (Mehar *et al*. 2018). Specifically, these distinguished properties of nanomaterials/nanostructures lead to their application in the field of nanoelectronics, nanodevices, nanosensors, nanoactuators, nanooscillators, electrical batteries, and nanocomposites (Sobhy and Radwan 2017). Therefore, it is important to investigate the accurate structural responses of such nanostructures under various loading and boundary conditions.

In the last few years, several numerical and analytical solution techniques have been employed to comprehend the mechanical behavior of nanoplate structures. In this context, Eringen (1983) developed a nonlocal elasticity theory to capture the small-scale effect. This non-local theory provides information about long-range interactions between atoms and internal scale lengths. Aghababaei and Reddy (2009) studied the relation between nonlocal classical, first, and third-order theories. The influence of nonlocal theory has been analyzed on deflection and natural frequency of the plate using the Nonlocal third-order shear deformation plate theory. Mantari and Monge (2016) investigated the nonlinear vibration response of skew nanoplates with small-scale effects. The differential quadrature method has been used in solving the governing equations.

Sobhy and Radwan (2017) investigated a new quasi 3D nonlocal plate theory for analyzing the vibration and buckling behavior of nanoplates in a thermal environment. Barretta *et al*. (2019) employed nonlocal formulation and elastic principal flexural curvatures and moments to investigate size effects in 2D Kirchhoff axisymmetric nano-plates. Barretta and Marotti de Sciarra (2019) presented a variational nonlocal gradient elasticity for nano-beams. In the continuation, Barretta *et al*. (2019) developed a stress-driven mixture model with the combination of local and

*Corresponding author, Ph.D.,
E-mail: ankit.gupta1@snu.edu.in

ISSN: 2287-237X (Print), 2287-2388 (Online)

nonlocal phases for Timoshenko nano-beams. Barretta and Marotti de Sciarra (2018) formulated constitutive boundary conditions to investigate the bounded nano-beams. The equivalence between the nonlocal strain gradient integral model of elasticity and the differential problem with constitutive boundary conditions has been discussed in detail. Authors (Sun and Zhang (2003), Zhu, *et al*. (2007), Liang *et al*. (2007), Ghabussi and Habibi (2020)) studied various molecular dynamics methods that have been taken into account atomic lengths and small-scale effects.

Arefi and Rabczuk (2019) employed the higher-order nonlocal shear deformation theory to carry out the electro-elastic analysis of a piezoelectric doubly curved nanoshell. Navier's method has been used for solving the governing equation. Gholami and Ansari (2018) also analyzed the imperfection sensitivity of vibration response and post-buckling behavior in pre-and post-buckled regions of nanoplate including surface effects. Karami and Janghorban (2019) investigated the free vibration of porous nanotubes with variable thickness using the Timoshenko beam model. The authors used the nonlocal strain gradient theory for the analysis. In the continuation, Karami, *et al*. (2019) investigated the free vibration response of doubly-curved nanoshells with temperature and porosity dependent material properties. Romano *et al*. (2017) formulated an integral constitutive law with explicit reference to the plane and straight nano-beams. Barretta *et al*. (2020) employed stress-driven nonlocal continuum mechanics to investigate the Size-dependent buckling of compressed Bernoulli-Euler nano-beams. Ebrahimi *et al*. (2019) employed the quasi-3D beam model beam theory with the conjunction of nonlocal strain gradient elasticity theory to investigate the vibration response of magneto-flexo-electric rotary porous nano-beams.

The forced vibrations of a porous functionally graded scale-dependent beam have been studied by Fenjan *et al*. (2020). The authors employed the differential quadrature method and nonlocal strain gradient theory for the analysis. In the continuation, the authors investigated the dynamic responses of porous piezoelectric and metal foam nano-size plates using four variables plate formulation (Fenjan *et al*. 2020). Batou *et al*. (2019) demonstrated the wave propagations in sigmoid functionally graded plates using new four unknown based higher order shear deformation theory. The dynamic instability analysis of electrostatic functionally graded doubly-clamped nano-actuators using Parameter expansion method by Sedighi *et al*. (2020). In addition to this, several reports are available dealing with the structural response of porous and nonporous graded structures using various solution methodologies and structural kinematics (Ebrahimi 2019b, Shariati *et al*. 2020, Ramirez *et al*. 2019, Sedighi *et al*. 2016).

In the view of the above discussion, it is observed that very few literature are available which deals with the structural response of porous FG nanoplate using non-polynomial higher-order shear deformation theory with the consideration of a small-scale effect. In addition to this, a generalized porosity model that is capable to demonstrate the effective material properties of porous FG plates including even and uneven distribution of pores is not

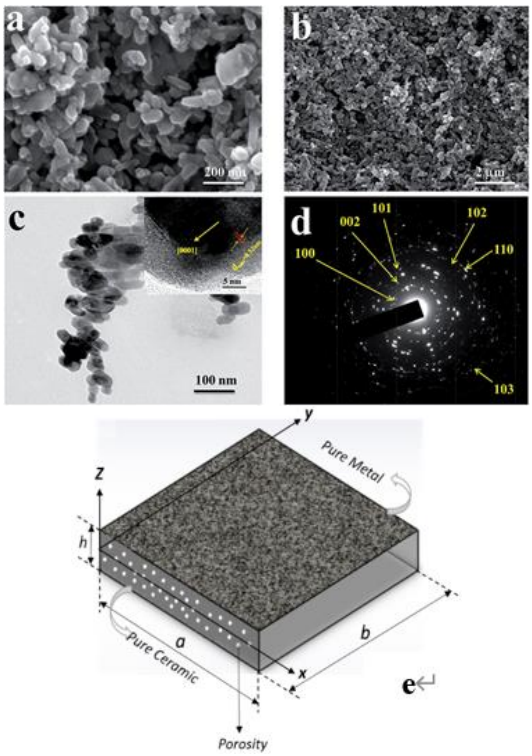

Fig. 1 (a) SEM image of ZnO nanoplates, (b) the same film at low magnification showing a porous film consisting of nanoplate nanostructures, (c) the low-resolution TEM image, (d) Electron diffraction pattern of the selected area (Patil *et al*. 2014) and (e) Geometric coordinates of FG porous Nanoplate

available in the literature. In addition to this, no literature is available which deals with FG porous nanoplate with partially supported boundary conditions. Therefore, the primary objective of the present study is to develop a nonpolynomial higher-order shear deformation theory with few numbers of unknowns compared to already existing deformation theories to analyze the vibration response of FG porous nanoplate. Apart from this, a generalized porosity model has been developed to incorporate the influence of porosity inclusion on the vibration response of FG nanoplates. The presented refined higher-order deformation theory consists of only four unknowns in which the out of plane displacement has been divided into bending and shear components. The shear-strain function used in the present study was initially given by Suganyadevi and Singh (2016) whereas, the small-scale effect in porous FG nanoplates have been captured using nonlocal elasticity theory. The influence of various parameters like a nonlocal parameter, porosity volume fraction, volume fraction index, thickness ratio on the natural frequency of porous FG nanoplates has been investigated.

The present paper consists of various sections. In subsequent sections, Sections 2 and 3 describe the mathematical formulations which further include Eringen's nonlocal theory, structural kinematics, constitutive relations, equations of motions, finite element formulation, and Navier's solution methods, etc. while section 4 comprises of

the results and discussion part of the work. The influence of various parameters on FG porous nanoplate has been shown in this section. At the last, section 5 summarizes the concluding remark of the present study.

2. Mathematical formulations

2.1. Eringen's nonlocal theory

According to Eringen's nonlocal theory (Eringen and Edelen 1972), it is supposed that the Stress at a point depends on the strain at all the points in the domain of the continuum so the influence of atomic forces and small scales are considered in constitutive equation as the material parameter. As per the experimental observations, Eringen proposed a constitutive model that expresses the nonlocal stress tensor at point *x* as (Eringen and Edelen 1972)

$$\sigma = \int_{v} \alpha(|x' - x|, \tau)\sigma_{ij}(x')dx' \tag{1}$$

$$\sigma_{ij} = C_{ijkl}\varepsilon_{kl} \tag{2}$$

where σ_{ij} is the Hookean stress tensor and $\alpha\left(|x' - x|\right)$ is the kernel function which is normalized over the volume of the body represents the nonlocal modulus, $|x' - x|$ is the distance, and τ is the material constant. In addition to this, the nonlocal theory also involves the spatial integral of the weighted average of the strains at all the points in the continuum body to the stress tensor at a point. To obtain the nonlocal constitutive relation in differential form, equations of motions have been obtained using nonlocal balance law (Eringen 1983)

$$t_{ij,j} + f_i = \rho\ddot{u}_i, \tag{3}$$

where *i, j* represents *x, y, z* and f_i , ρ *and* u_i represents the body force, mass density, and displacement vector respectively. By substituting Eq. (1) in Eq. (3), the constitutive relation's integral form obtained which is defined as

$$\sigma_{ij,j} + \left(1 - \mu\nabla^2\right)\left(f_i - \rho\ddot{u}\right) = 0 \tag{4}$$

The nonlocal constitutive equation given in integral form can also be expressed in the differential form proposed by Eringen as(Eringen and Edelen 1972)

$$(1 - \tau^2 L^2\nabla^2)\sigma = \sigma_{ij}, \qquad \tau^2 = \frac{\mu}{L^2} = \left(\frac{e_0\bar{a}}{L}\right)^2 \tag{5}$$

where $\mu = (e_0\bar{a})$, e_0 is a material constant and $\bar{a}$ and L are the internal and external characteristic lengths respectively.

2.2 Generalized porosity models

In the present paper, three porosity models have been employed to study the influence of porosity inclusion on the vibrational response of FG nanoplate. The first porosity model (PM1) was given by Ebrahimi and Jafari (2017)

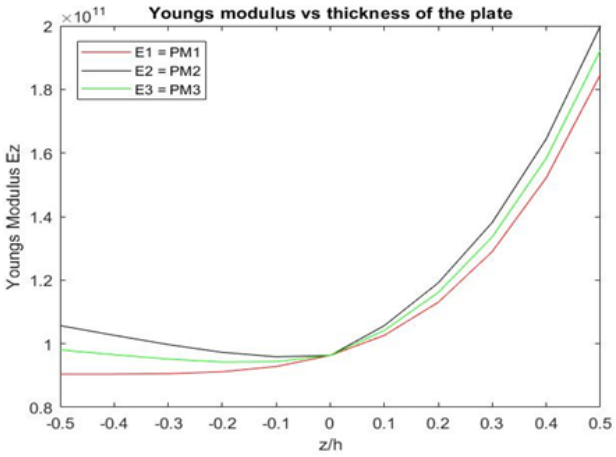

Fig. 2 E(z) variation with the thickness of FG Nanoplate

whereas the second porosity model (PM2) was given by the co-author (Gupta and Talha 2018b). In addition to this, a new generalized porosity governing model i.e. PM3 has been developed to study the even and uneven porous behavior of FG nanoplate. A specific attribute of the present model is that it includes both even and uneven distribution of porosity reported in the literature where λ (0 < λ < 1) is porosity volume fraction or porosity governing parameter (PGP). If λ = 0 it represents that the plate is nonporous whereas as the value of γ increases, porosity in the plate increases. Whereas B (0 < B <1) is porosity distribution factor. When B = 0 and B = 1 present the even and uneven porosity distribution respectively. The variation of Young's modulus with varying thickness has been presented in Fig. 2. The equations used to define the porosity models are as follows.

PM1

$$E(z) = E_m + (E_c - E_m)(0.5 + z/h)^P - \frac{\zeta}{2}(E_c + E_m) \tag{6}$$

PM2

$$E(z) = E_m + (E_c - E_m)(0.5 + z/h)^P - \log\left(1 + \frac{\lambda}{2}\right)[E_c + E_m]\left[1 - \frac{2|z|}{h}\right] \tag{7}$$

PM2

$$E(z) = E_m + (E_c - E_m)(0.5 + z/h)^P - \tan^{-1}(\kappa/2)[E_c + E_m]\left[1 - B\frac{2|z|}{h}\right] \tag{8}$$

where $E_m, E_c, \lambda, \zeta, \kappa, P$, h is the metal-ceramic Young's Modulus, porosity governing parameters (PGP) for PM1, PM2, PM3 models, volume fraction index, and thickness of the plate respectively. These porosity models have been used to calculate the effective material properties.

2.3 Theoretical formulations

A porous FG nanoplate with length *a*, breadth *b*, and thickness *h* has been used to study the vibration response. The geometry and coordinates of the FG plate have been shown in Fig. 1. The gradation in material properties from purely metal and ceramic has been governed by the power-

law distribution along the thickness direction. The effective bulk modulus (K) and shear modulus (G) is given by the Mori-Tanaka homogenization scheme. The equations involved in calculations of material properties is as follows (Belkorissat et al. (2015)

$$\frac{K-K_m}{K_c-K_m}=\frac{V_c}{1+(1-V_c)\frac{3(K_c-K_m)}{3(K_m+4K_m)}} \tag{9}$$

$$\frac{G-G_m}{G_c-G_m}=\frac{V_c}{1+(1-V_c)\frac{(G_c-G_m)}{(G_m+f_1)}} \tag{10}$$

$$f_1=\frac{G_m(9K_m+8G_m)}{6(K_m+2G_m)} \tag{11}$$

here $V_i(i=c,m)$, $K_i(i=c,m)$, $G_i(i=c,m)$ denotes the volume fraction, Bulk modulus, shear modulus of the ceramic, and metal respectively. The metal and ceramic phases are related by $V_c+V_m=1$ and V_c is expressed as follows (Thai and Choi (2013))

$$V_c(z)=\left(\frac{2z+h}{2h}\right)^P, \qquad P\geq 0 \tag{12}$$

where P in the above Eqs. (6) and (7) is Volume fraction index and effective mass density and Young's modulus is given by the rule of mixture

$$\rho=\rho_cV_c+\rho_mV_m \tag{13}$$

$$E(z)=E_mV_m+E_cV_c \tag{14}$$

2.3 Structural Kinematics

In the present study, refined Trigonometric higher-order deformation theory has been presented in which the out of plane displacement has been divided into bending and shear stress components. The displacement field of the present theory has been developed with the following attributes and assumptions:

• Infinitesimal strains are involved as the displacements are very small in comparison with the plate thickness.

• The transverse normal stress σ_z is negligible in comparison with in-plane stresses σ_x and σ_y. The transverse displacement u_3 includes two components of bending w_b and shear w_s. These components are functions of coordinates *x, y,* and time *t* only.

$$u_3(x,y,z,t)=w_b(x,y,t)+w_s(x,y,t)$$

• The bending parts of in-plane displacements are similar to those given by the classical plate theory (CPT).

• The shear parts of the in-plane displacements give rise to the nonlinear variations of shear strains whereas the transverse shear stresses vanish on the top and bottom surfaces of the plate.

Based on the above assumptions, the following displacement field has been obtained

$$U_i(x,y,z,t)=u_i(x,y,t)-zw_{bxi}-f(z)w_{sxi}(x,y,t)+\theta_{xi}(x,y,t) \tag{15}$$

where for

$$i=1,2;\ \{\theta_{xi}\}=0; \qquad i=3;\ \{w_{bxi},w_{sxi}\}=0$$

$$f(z)=\sin(\frac{\phi z}{h})\cos(\frac{\phi z}{h})-\frac{\phi z}{h}\cos(\phi), \quad \phi=2.3 \tag{16}$$

where u_1, u_2 and u_3 denote the displacements in x y and z directions respectively. For i = 3, u_3 θ_{xi} are w_b and w_s are bending and shear components of transverse displacements respectively and *h* is the plate thickness. The shear strain function *f*(*z*) used in the present theory was initially given by Sarangan and Singh (2016) for the laminated composite plates. The nonzero strains are associated with the above displacement fields are as follows (Belkorissat et al. 2015).

$$\begin{aligned}
\varepsilon_x&=\frac{\partial u}{\partial x}=\left\{\frac{\partial u}{\partial x}-z\frac{\partial^2 w_b}{\partial x^2}-f(z)\left(\frac{\partial^2 w_s}{\partial x^2}\right)\right\}\\
\varepsilon_y&=\frac{\partial v}{\partial y}=\left\{\frac{\partial v}{\partial y}-z\frac{\partial^2 w_b}{\partial y^2}-f(z)\left(\frac{\partial^2 w_s}{\partial y^2}\right)\right\}\\
\gamma_{xy}&=\frac{\partial u}{\partial y}+\frac{\partial v}{\partial x}=\left\{\frac{\partial u}{\partial y}+\frac{\partial v}{\partial x}-2z\frac{\partial^2 w_b}{\partial x\partial y}-2f(z)\left(\frac{\partial^2 w_s}{\partial x\partial y}\right)\right\}\\
\gamma_{xz}&=\frac{\partial u}{\partial z}+\frac{\partial w}{\partial x}=\left\{(g(z))\frac{\partial w_s}{\partial x}\right\}\\
\gamma_{yz}&=\frac{\partial v}{\partial z}+\frac{\partial w}{\partial y}=\left\{(g(z))\frac{\partial w_s}{\partial y}\right\}
\end{aligned} \tag{17}$$

$$g(z)=1-f'(z) \tag{18}$$

2.4 Constitutive relations

Eringen's nonlocal theory (Eringen and Edelen 1972) has been employed in the constitutive relations to incorporate the small-scale effects. Eq. (8) has been used to incorporate the nonlocality into the constitutive relation for elastic porous FG nanoplate. The stress-strain relations for the present work are as follows

$$(1-\mu\nabla^2)\{\sigma\}^{NLP}=\left[C_{ij}\right]\{\varepsilon\} \tag{19a}$$

where NLP defines Nonlocal stresses and Eq. (19a) can be written in expanded form as in Eq. (19b)

$$\begin{Bmatrix}\sigma_x\\ \sigma_y\\ \tau_{xy}\\ \tau_{xz}\\ \tau_{yz}\end{Bmatrix}-\mu\nabla^2\begin{Bmatrix}\sigma_x\\ \sigma_y\\ \tau_{xy}\\ \tau_{xz}\\ \tau_{yz}\end{Bmatrix}=\begin{bmatrix}C_{11}&C_{12}&0&0&0\\ C_{12}&C_{22}&0&0&0\\ 0&0&C_{44}&0&0\\ 0&0&0&C_{55}&0\\ 0&0&0&0&C_{66}\end{bmatrix}\begin{Bmatrix}\frac{\partial u}{\partial x}-z\frac{\partial^2 w_b}{\partial x^2}-f(z)\left(\frac{\partial^2 w_s}{\partial x^2}\right)\\ \frac{\partial v}{\partial y}-z\frac{\partial^2 w_b}{\partial y^2}-f(z)\left(\frac{\partial^2 w_s}{\partial y^2}\right)\\ \frac{\partial u}{\partial y}+\frac{\partial v}{\partial x}-2z\frac{\partial^2 w_b}{\partial x\partial y}-2f(z)\left(\frac{\partial^2 w_s}{\partial x\partial y}\right)\\ (g(z))\frac{\partial w_s}{\partial x}\\ (g(z))\frac{\partial w_s}{\partial x}\end{Bmatrix} \tag{19b}$$

$$C_{11} = C_{22} = \frac{E(z)}{1-\nu(z)^2}, \quad C_{12} = \frac{\nu E(z)}{1-\nu(z)^2}, \quad C_{44} = C_{55} = C_{66} = \frac{E(z)}{2(1+\nu(z))} \tag{20}$$

where $\sigma_i\ (i = x, y)$ and $\tau_{xy}, \tau_{xz}, \tau_{zy}$ are the stress and strain components respectively while C_{ij} denotes the stiffness coefficients.

2.5 Equations of Motion

Hamilton's principle has been used to derive the equations of motions. The governing equation for the trigonometric higher-order deformation theory has been derived using the dynamic version of the virtual displacement principle. The derivation of energy equations have been carried out in various steps which are as follows

$$0 = \int_0^T (\delta U + \delta V - \delta K)dt \tag{21}$$

2.5.1 Strain energy

Strain energy variation can be calculated using the given formula in the FG plate.

$$\delta U = \int_V (\sigma_x \delta\varepsilon_x + \sigma_y \delta\varepsilon_y + \sigma_{xy}\delta\gamma_{xy} + \sigma_{xz}\delta\gamma_{xz} + \sigma_{yz}\delta\gamma_{yz})dAdz \tag{22}$$

$$\delta U = \int_A [N_x\delta\varepsilon_x^0 + N_y\delta\varepsilon_y^0 + N_{xy}\delta\varepsilon_{xy}^0 + M_x^b\delta k_x^b + M_y^b\delta k_y^b + M_{xy}^b\delta k_{xy}^b + M_x^s\delta k_x^s + M_y^s\delta k_y^s + M_{xy}^s\delta k_{xy}^s + S_{yz}^s\delta k_{yz}^s + S_{xz}^s\delta k_{xz}^s]dA \tag{23}$$

where *N*, *M*, and *S* are the stress resultants defined by

$$(N_i, M_i^b, M_i^s) = \int_{-h/2}^{h/2}(1, z, f)\sigma_i dz,\ (i = x, y, xy), \quad S = \int_{-h/2}^{h/2} g\sigma_i dz,\ (i = xz, yz) \tag{24}$$

The variation of Kinetic energy of the plate is expressed as

$$\begin{aligned}\delta K &= \int_{-h/2}^{h/2}\int_A [\ddot{u}\delta u + \ddot{v}\delta v + \ddot{w}\delta w]\rho(z)dAdz \\ &= \int_A \{I_0[\ddot{u}_0\delta u_0 + \ddot{v}_0\delta v_0 + (\ddot{w}_b + \ddot{w}_s)(\delta w_b + \delta w_s)] \\ &\quad - I_1(\ddot{u}_0\frac{\partial\delta w_b}{\partial x} + \frac{\partial\ddot{w}_b}{\partial x}\delta u_0 + \ddot{v}_0\frac{\partial\delta w_b}{\partial y} + \frac{\partial\ddot{w}_b}{\partial y}\delta v_0) \\ &\quad - J_1(\ddot{u}_0\frac{\partial\delta w_s}{\partial x} + \frac{\partial\ddot{w}_s}{\partial x}\delta u_0 + \ddot{v}_0\frac{\partial\delta w_s}{\partial y} + \frac{\partial\ddot{w}_s}{\partial y}\delta v_0) \\ &\quad + I_2(\frac{\partial\ddot{w}_b}{\partial x}\frac{\partial\delta w_b}{\partial x} + \frac{\partial\ddot{w}_b}{\partial y}\frac{\partial\delta w_b}{\partial y}) + K_2(\frac{\partial\ddot{w}_s}{\partial x}\frac{\partial\delta w_s}{\partial x} + \frac{\partial\ddot{w}_s}{\partial y}\frac{\partial\delta w_s}{\partial y}) \\ &\quad + J_2(\frac{\partial\ddot{w}_b}{\partial x}\frac{\partial\delta w_s}{\partial x} + \frac{\partial\ddot{w}_s}{\partial x}\frac{\partial\delta w_b}{\partial x} + \frac{\partial\ddot{w}_b}{\partial y}\frac{\partial\delta w_s}{\partial y} + \frac{\partial\ddot{w}_s}{\partial y}\frac{\partial\delta w_b}{\partial y})\}dA\end{aligned} \tag{25}$$

Here the dot-superscript indicates the differentiation with respect to time and mass inertia defined as

$$(I_0, I_1, J_1, I_2, J_2, K_2) = \int_{-\frac{h}{2}}^{+\frac{h}{2}}\left(1, z, f, z^2, zf, f^2\right)\rho(z)dz \tag{26}$$

Substituting the expressions for δU and δK from Eqs. (23) and (25) into Eq. (21) and integrating by parts, and collecting the coefficients of δu_0, δv_0, δw_b and δw_s, the following equations of motion of the proposed theory are obtained as

$$\begin{aligned}
\delta u &: \left(\frac{\partial N_x}{\partial x} + \frac{\partial N_{xy}}{\partial y}\right) = \left\{I_0\ddot{u}_0 - I_1\frac{\partial\ddot{w}_b}{\partial x} - J_1\frac{\partial\ddot{w}_s}{\partial x}\right\} \\
\delta v &: \left(\frac{\partial N_{xy}}{\partial x} + \frac{\partial N_y}{\partial y}\right) = \left\{I_0\ddot{v}_0 - I_1\frac{\partial\ddot{w}_b}{\partial y} - J_1\frac{\partial\ddot{w}_s}{\partial y}\right\} \\
\delta w_b &: \left(\frac{\partial^2 M_x^b}{\partial x^2} + \frac{\partial^2 M_y^b}{\partial y^2} + 2\frac{\partial^2 M_{xy}^b}{\partial x\partial y}\right) = \left\{I_0(\ddot{w}_b + \ddot{w}_s) + I_1\left(\frac{\partial\ddot{u}_0}{\partial x} + \frac{\partial\ddot{v}_0}{\partial y}\right) - I_2\nabla^2\ddot{w}_b - J_2\nabla^2\ddot{w}_s\right\} \\
\delta w_s &: \left(\frac{\partial^2 M_x^s}{\partial x^2} + \frac{\partial^2 M_y^s}{\partial y^2} + 2\frac{\partial^2 M_{xy}^s}{\partial x\partial y} + \frac{\partial S_{xz}^s}{\partial x} + \frac{\partial S_{yz}^s}{\partial y}\right) = \left\{I_0(\ddot{w}_b + \ddot{w}_s) + J_1\left(\frac{\partial\ddot{u}_0}{\partial x} + \frac{\partial\ddot{v}_0}{\partial y}\right) - J_2\nabla^2\ddot{w}_b - K_2\nabla^2\ddot{w}_s\right\}
\end{aligned} \tag{27}$$

Substituting Eqs. (17) and (19) into Eq. (24) and integrating through the thickness of the plate, the stress resultants are related to the generalized displacements (of δu_0, δv_0, δw_b and δw_s) by the relations

$$\begin{Bmatrix} N \\ M^b \\ M^s \end{Bmatrix} - \mu\nabla^2\begin{Bmatrix} N \\ M^b \\ M^s \end{Bmatrix} = \begin{bmatrix} P & Q & Q^s \\ Q & R & R^s \\ Q^s & R^s & T^s \end{bmatrix}\begin{Bmatrix} \varepsilon \\ k^b \\ k^s \end{Bmatrix}, \quad S - \mu\nabla^2 = P^s\gamma, \tag{28}$$

where

$$N = \left\{N_x, N_y, N_{xy}\right\}^t,\ M^b = \left\{M_x^b, M_y^b, M_{xy}^b\right\}^t,\ M^s = \left\{M_x^s, M_y^s, M_{xy}^s\right\}^t$$
$$\varepsilon = \left\{\varepsilon_x^0, \varepsilon_y^0, \varepsilon_{xy}^0\right\}^t,\ k^b = \left\{k_x^b, k_y^b, k_{xy}^b\right\}^t,\ k^s = \left\{k_x^s, k_y^s, k_{xy}^s\right\}^t \tag{29a}$$

$$P = \begin{bmatrix} P_{11} & P_{12} & 0 \\ P_{12} & P_{22} & 0 \\ 0 & 0 & P_{66} \end{bmatrix},\quad Q = \begin{bmatrix} Q_{11} & Q_{12} & 0 \\ Q_{12} & Q_{22} & 0 \\ 0 & 0 & Q_{66} \end{bmatrix},\quad R = \begin{bmatrix} R_{11} & R_{12} & 0 \\ R_{12} & R_{22} & 0 \\ 0 & 0 & R_{66} \end{bmatrix},$$
$$Q^s = \begin{bmatrix} Q_{11}^s & Q_{12}^s & 0 \\ Q_{12}^s & Q_{22}^s & 0 \\ 0 & 0 & Q_{66}^s \end{bmatrix},\quad R^s = \begin{bmatrix} R_{11}^s & R_{12}^s & 0 \\ R_{12}^s & R_{22}^s & 0 \\ 0 & 0 & R_{66}^s \end{bmatrix},\quad H^s = \begin{bmatrix} H_{11}^s & H_{12}^s & 0 \\ H_{12}^s & H_{22}^s & 0 \\ 0 & 0 & H_{66}^s \end{bmatrix}, \tag{29b}$$

$$S = \left\{S_{xz}^s, S_{yz}^s\right\}^t,\ \gamma = \left\{\gamma_{xz}^s, \gamma_{yz}^s\right\}^t,\quad P^s = \begin{bmatrix} P_{44}^s & 0 \\ 0 & P_{55}^s \end{bmatrix} \tag{29c}$$

where *P*, *Q*, *R*, and *H* are the plate stiffness which are defined by

$$\begin{Bmatrix} P_{11} & Q_{11} & R_{11} & Q_{11}^s & R_{11}^s & T_{11}^s \\ P_{12} & Q_{12} & R_{12} & Q_{12}^s & R_{12}^s & T_{12}^s \\ P_{66} & Q_{66} & R_{66} & Q_{66}^s & R_{66}^s & T_{66}^s \end{Bmatrix} = \int_{-h/2}^{h/2} C_{11}(1, z, z^2, f(z), zf(z), f^2(z))\begin{Bmatrix} 1 \\ \nu \\ \frac{1-\nu}{2} \end{Bmatrix}dz,$$
$$(P_{22}, Q_{22}, R_{22}, Q_{22}^s, R_{22}^s, T_{22}^s) = (P_{11}\ Q_{11}\ R_{11}\ Q_{11}^s\ R_{11}^s\ T_{11}^s),$$
$$P_{44}^s = P_{55}^s = \int_{-h/2}^{h/2} C_{44}\left[g(z)\right]^2 dz \tag{30}$$

Substituting from Eq. (19) into Eq. (18), we obtain the following equation

$$P_{11}\frac{\partial^2 u_0}{\partial x^2}+P_{66}\frac{\partial^2 u_0}{\partial y^2}+(P_{12}+P_{66})\frac{\partial^2 v_0}{\partial x\partial y}-Q_{11}\frac{\partial^3 w_b}{\partial x^3}-(Q_{12}+2Q_{66})\frac{\partial^3 w_b}{\partial x\partial y^2}$$
$$-Q^s_{11}\frac{\partial^3 w_s}{\partial x^3}-(Q^s_{12}+2Q^s_{66})\frac{\partial^3 w_s}{\partial x\partial y^2}=(1-\mu\nabla^2)\left[I_0\ddot{u}_0-I_1\frac{\partial\ddot{w}_b}{\partial x}-J_1\frac{\partial\ddot{w}_s}{\partial x}\right] \quad (31a)$$

$$P_{22}\frac{\partial^2 v_0}{\partial x^2}+P_{66}\frac{\partial^2 v_0}{\partial y^2}+(P_{12}+P_{66})\frac{\partial^2 u_0}{\partial x\partial y}-Q_{22}\frac{\partial^3 w_b}{\partial y^3}-(Q_{12}+2Q_{66})\frac{\partial^3 w_b}{\partial x^2\partial y}$$
$$-Q^s_{22}\frac{\partial^3 w_s}{\partial y^3}-(Q^s_{12}+2Q^s_{66})\frac{\partial^3 w_s}{\partial x^2\partial y}=(1-\mu\nabla^2)\left[I_0\ddot{v}_0-I_1\frac{\partial\ddot{w}_b}{\partial y}-J_1\frac{\partial\ddot{w}_s}{\partial y}\right] \quad (31b)$$

$$P_{22}\frac{\partial^2 v_0}{\partial x^2}+P_{66}\frac{\partial^2 v_0}{\partial y^2}+(P_{12}+P_{66})\frac{\partial^2 u_0}{\partial x\partial y}-Q_{22}\frac{\partial^3 w_b}{\partial y^3}-(Q_{12}+2Q_{66})\frac{\partial^3 w_b}{\partial x^2\partial y}$$
$$-Q^s_{22}\frac{\partial^3 w_s}{\partial y^3}-(Q^s_{12}+2Q^s_{66})\frac{\partial^3 w_s}{\partial x^2\partial y}=(1-\mu\nabla^2)\left[I_0\ddot{v}_0-I_1\frac{\partial\ddot{w}_b}{\partial y}-J_1\frac{\partial\ddot{w}_s}{\partial y}\right] \quad (31c)$$

$$Q^s_{11}\frac{\partial^3 u_0}{\partial x^3}+(Q^s_{12}+2Q^s_{66})\frac{\partial^3 u_0}{\partial x\partial y^2}+(Q^s_{12}+2Q^s_{66})\frac{\partial^3 v_0}{\partial x^2\partial y}+Q^s_{22}\frac{\partial^3 v_0}{\partial y^3}$$
$$-R^s_{11}\frac{\partial^4 w_b}{\partial x^4}-2(R^s_{12}+2R^s_{66})\frac{\partial^4 w_b}{\partial x^2\partial y^2}-R^s_{22}\frac{\partial^4 w_b}{\partial y^4}$$
$$-T^s_{11}\frac{\partial^4 w_s}{\partial x^4}-2(T^s_{12}+2T^s_{66})\frac{\partial^4 w_s}{\partial x^2\partial y^2}-T^s_{22}\frac{\partial^4 w_s}{\partial y^4}+P^s_{44}\frac{\partial^2 w_s}{\partial x^2}+P^s_{55}\frac{\partial^2 w_s}{\partial y^2}$$
$$=(1-\mu\nabla^2)\left[I_0(\ddot{w}_b+\ddot{w}_s)+J_1(\frac{\partial\ddot{u}_0}{\partial x}+\frac{\partial\ddot{v}_0}{\partial x})-J_2\nabla^2\ddot{w}_b-K_2\nabla^2\ddot{w}_s\right] \quad (31d)$$

2.6 Closed-form solution for Porous FG nanoplate

In the present study, the governing equations which are derived using Hamilton's principle are solved using Navier's method for simply supported boundary conditions. The employed boundary conditions are as follows.

$$v_0=w_b=w_s=\frac{\partial w_s}{\partial y}=N_x=M^b_x=M^s_x=0 \ \ at\ x=0,a$$
$$u_0=w_b=w_s=\frac{\partial w_s}{\partial y}=N_y=M^b_y=M^s_y=0 \ \ at\ y=0,a \quad (32)$$

Following the Navier solution procedure, we assume the following solution form for δu_0, δv_0, δw_b and δw_s that satisfies the boundary conditions given in Eq. (31)

$$u(x,y,t)=\sum_{m=1}^{\infty}\sum_{n=1}^{\infty}U_{mn}e^{i\omega t}\cos\alpha x\sin\beta y \quad (33a)$$

$$v(x,y,t)=\sum_{m=1}^{\infty}\sum_{n=1}^{\infty}V_{mn}e^{i\omega t}\sin\alpha x\cos\beta y \quad (33b)$$

$$w_b(x,y,t)=\sum_{m=1}^{\infty}\sum_{n=1}^{\infty}W_{bmn}e^{i\omega t}\sin\alpha x\sin\beta y \quad (33c)$$

$$w_s(x,y,t)=\sum_{m=1}^{\infty}\sum_{n=1}^{\infty}W_{smn}e^{i\omega t}\sin\alpha x\sin\beta y \quad (33d)$$

where U_{mn}, V_{mn}, W_{bmn} and W_{smn} are arbitrary parameters to be defined, ω is Eigen frequency associated with (m, n) Eigenmode, and $\alpha = m\pi / a$ and $\beta = n\pi / b$.

Substituting Eqs. (24) into Eq. (22), the analytical solutions can be obtained from

$$\left(\begin{bmatrix}a_{11}&a_{12}&a_{13}&a_{14}\\a_{21}&a_{22}&a_{23}&a_{24}\\a_{31}&a_{32}&a_{33}&a_{34}\\a_{41}&a_{42}&a_{43}&a_{44}\end{bmatrix}-\omega^2\begin{bmatrix}m_{11}&0&0&0\\0&m_{22}&0&0\\0&0&m_{33}&m_{34}\\0&0&m_{43}&m_{34}\end{bmatrix}\right)\begin{Bmatrix}U_{mn}\\V_{mn}\\W_{bmn}\\W_{smn}\end{Bmatrix}=\begin{Bmatrix}0\\0\\0\\0\end{Bmatrix} \quad (34)$$

where

$$\begin{aligned}
a_{11}&=P_{11}\alpha^2+P_{66}\beta^2\\
a_{12}&=\alpha\beta(P_{12}+P_{66})\\
a_{13}&=-\alpha[Q_{11}\alpha^2+(Q_{12}+2Q_{66})\beta^2]\\
a_{14}&=-\alpha[Q^s_{11}\alpha^2+(Q^s_{12}+2Q^s_{66})\beta^2]\\
a_{22}&=P_{66}\alpha^2+P_{22}\beta^2\\
a_{23}&=-\beta[(Q_{12}+2Q_{66})\alpha^2+Q_{22}\beta^2]\\
a_{24}&=-\beta[(Q^s_{12}+2Q^s_{66})\alpha^2+Q^s_{22}\beta^2]\\
a_{33}&=R_{11}\alpha^4+2(R_{12}+2R_{66})\alpha^2\beta^2+R_{22}\beta^4\\
a_{34}&=R^s_{11}\alpha^4+2(R^s_{12}+2R^s_{66})\alpha^2\beta^2+R^s_{22}\beta^4\\
a_{44}&=T^s_{11}\alpha^4+2(T^s_{12}+2T^s_{66})\alpha^2\beta^2+T^s_{22}\beta^4+P^s_{55}\alpha^2+P^s_{44}\beta^2
\end{aligned} \quad (35)$$

$$\begin{aligned}
m_{11}&=m_{22}=\lambda I_0\\
m_{33}&=m_{11}+\lambda I_2(\alpha^2+\beta^2))\\
m_{34}&=m_{11}+\lambda J_2(\alpha^2+\beta^2)\\
m_{44}&=m_{11}+\lambda k_2(\alpha^2+\beta^2)\\
\lambda&=1+\mu(\alpha^2+\beta^2)
\end{aligned} \quad (36)$$

3. Finite element formulation

3.1. Continuity requirement

C^1 continuous element is being required for the displacement field as stated in Eq. (15). As it is well known that there are difficulties associated with C^1-continuous finite element so to reduce the continuity requirement to C^0, first derivatives of shear and bending displacements are considered as a separate degree of freedom. Hence the modified displacement field can be written as:

$$\begin{aligned}
U_1(x,y,z,t)&=u_0(x,y,t)-z\alpha_x(x,y,t)+f(z)\beta_x(x,y,t)\\
U_2(x,y,z,t)&=v_0(x,y,t)-z\alpha_y(x,y,t)+f(z)\beta_y(x,y,t)\\
U_3(x,y,z,t)&=w_b(x,y,t)+w_s(x,y,t)
\end{aligned} \quad (36)$$

where

$$\alpha_x=\frac{\partial w_b}{\partial x},\alpha_y=\frac{\partial w_b}{\partial y},\beta_x=\frac{\partial^2 w_s}{\partial x^2},\beta_y=\frac{\partial^2 w_s}{\partial y^2},u,v,w_b,w_s$$

are the degrees of freedom.

3.2 Element type

In Finite element formulation on FG porous nanoplate, the plate is discretized using a C^0-continuous Lagrangian

quadrilateral four-noded element with eight degrees of freedom per node. Displacement vector and element geometry can be expressed in terms of shape functions given as:

$$u = NU_0, v = NV_0, w_b = NW_b, w_s = NW_s$$

$$\delta(x,y,z,t) = \begin{Bmatrix} u \\ v \\ w_b \\ w_s \end{Bmatrix} = \begin{bmatrix} N & 0 & -zN_{,x} & f(z)N_{,xx} \\ 0 & N & -zN_{,y} & f(z)N_{,yy} \\ 0 & 0 & N & N \end{bmatrix} \delta^e$$

where,

$$\delta^e = \begin{bmatrix} U_0 \\ V_0 \\ W_b \\ W_s \end{bmatrix} \tag{38}$$

and N, u, v, w_b, w_s are the shape function vector and displacement vector in different directions.

3.3 Strain energy of the plate

The strain energy formula for i[th] element of FG nanoplate is given by:

$$\Pi^e = \frac{1}{2}\int_v \{\varepsilon\}^T{}_j \{\sigma\}^{NLP}{}_j \, dV$$

$$\Pi^e = \frac{1}{2}\int_v \{\varepsilon\}^T{}_j \left[C_{ij}\right]\{\varepsilon\}_j \, dV\,'$$

$$\Pi^e = \frac{1}{2}\int_v \left[\frac{1}{2}\left(\{\varepsilon\}^T{}_j [\psi]\{\varepsilon\}_i\right)\right] dV$$

where,

$$[\psi] = \int_{-h/2}^{h/2} [\chi]^T [C][\chi] dz \tag{39}$$

So final strain energy equation becomes

$$\Pi^e = \frac{1}{2}\int_v \left[\frac{1}{2}\left(\{\varepsilon\}^T{}_j [\chi]^T [C][\chi]\{\varepsilon\}_i\right)\right] dV \tag{40}$$

where,

$$[\chi] = \begin{bmatrix} 1&0&0&0&z&0&0&f(z)&0&0&0&0&0&0&0 \\ 0&1&0&0&0&z&0&0&f(z)&0&0&0&0&0&0 \\ 0&0&0&0&0&0&0&0&0&0&0&0&0&0&0 \\ 0&0&1&0&0&0&0&0&0&0&1&0&0&0&0 \\ 0&0&0&1&0&0&0&0&0&0&0&1&0&0&0 \\ 0&0&0&0&0&0&z&0&0&f(z)&0&0&0&0&0 \end{bmatrix}$$

3.4 Kinetic energy

The variation of Kinetic energy of the FG nanoplate is expressed as

$$\delta K = \frac{1}{2}\int_v \rho\left\{\dot{\bar{U}}\right\}^T \left\{\dot{\bar{U}}\right\} dV \tag{41}$$

where $'\rho', \{\bar{U}\}$ are the density and the global displacement vector of the FG plate and the global displacement field is presented as $\{\bar{U}\} = [\bar{T}]\{U\}$, where $[\bar{T}]$ is the function of thickness coordinate

$$[\bar{T}] = \begin{bmatrix} 1&0&0&-z&0&0&f(z)&0 \\ 0&1&0&0&-z&0&0&f(z) \\ 0&0&1&0&0&0&0&1 \end{bmatrix}, \tag{42}$$

$$\delta K = \frac{1}{2}\int_V (\int_z \rho\{\dot{U}\}^T [\bar{T}]^T [\bar{T}]\{\dot{U}\} dz) dV$$

$$\delta K = \frac{1}{2}\int_A (\{\dot{U}\}^T [m]\{\dot{U}\} dA) \tag{43}$$

where, $[m]^{(e)}$ is the inertial elemental mass matrix.

3.5 Governing Equation

The governing equation for free vibration analysis of FGM plate has been inferred using the variational principle as given below:

$$([K] - \lambda[M])\{\bar{U}\} = 0 \tag{44}$$

where ω is defined as the frequency of natural vibration. Where $[M]$, $[K]$, are global mass matrix, global linear stiffness matrix, respectively.

4. Results and duscussions

In the present section, the vibration analysis of porous FG plate with the conjunction of small-scale effects has been carried out. Ti-6Al-4V/ZrO_2 has been used as a FG material for the analysis. The material properties of the Ti-6Al-4V/ZrO_2 are given in Table 1.

The non-dimensional fundamental frequency has been used as $\omega = \varpi h\sqrt{\frac{\rho}{G}}$ where ω is the non-dimensional frequency parameter, ρ and G are the mass density and shear modulus respectively.

The subsequent section has been divided into two parts. In the first section, a comparison study has been carried out while in the second section, a detailed parametric study has been done.

4.1 Comparison study

Two test examples have been presented in this section to establish the accuracy and applicability of the present theory to predict the realistic vibration response of the FG

Table 1 Material Properties

S. No.	*Properties*	*E (GPa)*	ρ (kg/m^3)	*ν*
1	Ti-6Al4V	105.7	4429	0.3
2	ZrO_2	200	5700	0.3
3	SUS304	201	8166	0.3
4	Si3N4	348	2370	0.3

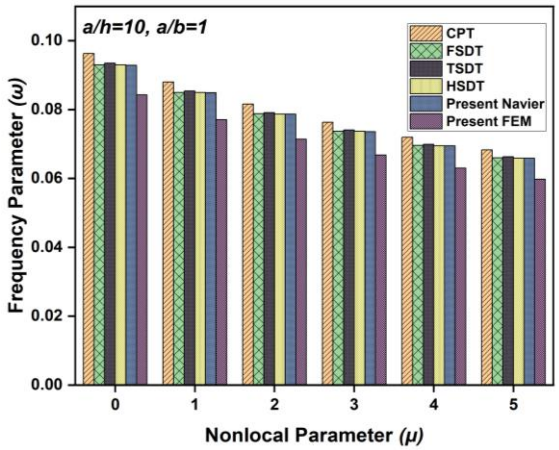

Fig. 3 VFP[$] for nonlocal parameter (μ) at $a/b = 1$

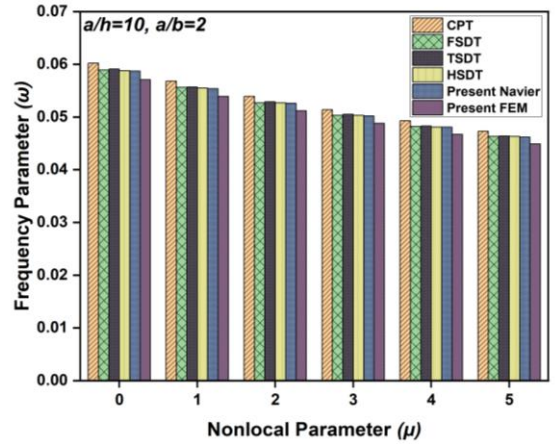

Fig. 4 VFP for nonlocal parameter μ at $a/b = 2$

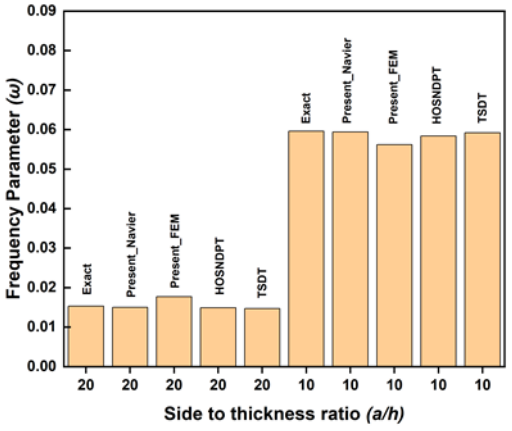

Fig. 5 Comparative study of Trigonometric theory with HSDT's at P = 1

nanoplates. Comparative studies have been carried out with the available existing results in the literature. The description of the material properties used in the analysis is provided in Table 1. The numerical results are presented in graphical and as well as in tabular forms.

Example 1: In the first example, the vibration response of SUS304/Si_3N_4 FG nanoplates has been investigated using the proposed refined trigonometric shear deformation theory. The results obtained from the present solution comprising of both Navier as well as finite element method have been compared with the results given by Belkorissat *et al*. (2015). They have used the four-variable model using nonlocal theory within the conjunction of Navier's method. The non-dimensional frequency parameter i.e., $\omega = \varpi h\sqrt{\frac{\rho}{G}}$ has been used. The variation of the frequency parameter with the nonlocal parameter *(μ)* and side to thickness ratio *(a/h)* has been observed in Figs. 3 and 4. The nonlocal parameter *(μ)* has been varied from 0 to 5 for different side to thickness ratios *(a/h)*. It is evident from the reported results that the proposed trigonometric theory is in good agreement with the nonlocal refined four variable models.

Example 2: In the second example, the comparative study of developed theory with other higher-order shear deformation theories and exact solution have been carried out as shown in Fig. 5. The obtained results are compared with the results given by Jha *et al*. (2013) for a/h = 10 and 20. It is observed that the percentage difference between the present results and the referred results is approximately 1% to 2%. The reported results showed that the Trigonometric theory is closer to the values of fundamental frequency obtained using HSDT.

4.2 Parametric study

Considering the preceding section, it can be noticed that the developed theory delivers results that are in good agreement with other higher-order shear deformation theories and 3D exact solution of the vibrated FG plate. In the consequent section, the parametric studies have been carried out to investigate the influence of various parameters such as aspect ratio *(a/b)*, volume fraction index *(P)*, Nonlocal parameter *(μ)*, side to thickness ratio *(a/h)*, etc. on the vibration response of Ti-6Al-4V/Zr O_2 FG nanoplate. The further study has been divided into two parts, the first one deals with Navier's solution and the second one with the FEM solution.

4.3 Case I: Closed form solution

The governing equation derived using Hamilton's principle in the preceding section has been solved using Navier's method. The effect and influence of various parameters like side to thickness ratios (a/h), Non-local parameter (μ), porosity volume fractions, etc. have been observed and reported.

4.3.1 Influence of side to thickness ratio (a/h) with varying Nonlocal parameter (μ)

In Tables 2 and 3, the fundamental frequency of Ti-6Al-4V/ZrO_2 FG square nanoplate at volume fraction index of 1 has been reported for different side to thickness ratios *(a/h)* and porosity volume fraction in conjugation with varying nonlocal parameter *(μ)*. In porosity models 1 and 2, it has been found that the fundamental frequency decreases with the increase in porosity volume fraction and nonlocal parameter *(μ)*.

It is evident from the results that as the nonlocal parameer

Table 2 Variation of frequency parameter with μ and *a/h* at (PM1, *P* = 1, *a/b* = 1)

Ti-6Al-4V/ZrO_2		**Nonlocal parameter (μ)**						
a/h	**ζ**	**0**	**1**	**2**	**3**	**4**	**5**	**% diff1#**
	0	0.3402	0.3109	0.2880	0.2696	0.2543	0.2413	(29.0711)
	0.1	0.3215	0.2938	0.2723	0.2548	0.2404	0.2281	(29.0513)
5	**% diff***	(5.4968)	(5.5002)	(5.4514)	(5.4896)	(5.4660)	(5.4704)	
	0.2	0.3016	0.2756	0.2554	0.2390	0.2254	0.2139	(29.0782)
	% diff *	(11.3463)	(11.3541)	(11.3194)	(11.3501)	(11.3645)	(11.3552)	
	0	0.0909	0.0831	0.0770	0.0721	0.0680	0.0645	(29.0429)
	0.1	0.0859	0.0785	0.0728	0.0681	0.0642	0.0610	(28.9872)
10	**% diff***	(5.5006)	(5.5355)	(5.4545)	(5.5479)	(5.5882)	(5.4264)	
	0.2	0.0806	0.0736	0.0682	0.0639	0.0602	0.0572	(29.0323)
	% diff*	(11.3311)	(11.4320)	(11.4286)	(11.3731)	(11.4706)	(11.3178)	
	0	0.0230	0.0211	0.0195	0.0183	0.0172	0.0163	(29.1304)
	0.1	0.0218	0.0199	0.0184	0.0173	0.0163	0.0155	(28.8991)
20	**% diff***	(5.2174)	(5.6872)	(5.6410)	(5.4645)	(5.2326)	(4.9080)	
	0.2	0.0204	0.0187	0.0173	0.0162	0.0153	0.0145	(28.9216)
	% diff*	(11.3043)	(11.3744)	(11.2821)	(11.4754)	(11.0465)	(11.0429)	

$*\%diff = (\lambda(0) - \lambda(0.1 \text{ or } 0.2)) * 100 / \lambda(0)$, $\#\%diff1 = (\mu(0) - \mu(5)) * 100 / \mu(0)$

Table 3 Variation of frequency parameter with μ and a/h at (PM2, P = 1, *a/b* = 1)

Ti-6Al-4V/ZrO_2		**Nonlocal parameter (μ)**						
a/h	**λ**	**0**	**1**	**2**	**3**	**4**	**5**	**% diff1**
	0	0.3402	0.3109	0.2880	0.2696	0.2543	0.2413	(29.0711)
	0.1	0.3264	0.2983	0.2764	0.2587	0.2440	0.2316	(29.0441)
5	**% diff**	(4.0564)	(4.0528)	(4.0278)	(4.0430)	(4.0503)	(4.0199)	
	0.2	0.3124	0.2855	0.2645	0.2476	0.2335	0.2216	(29.0653)
	% diff	(8.1717)	(8.1698)	(8.1597)	(8.1602)	(8.1793)	(8.1641)	
	0	0.0909	0.0831	0.0770	0.0721	0.0680	0.0645	(29.0429)
	0.1	0.0874	0.0798	0.0740	0.0692	0.0653	0.0620	(29.0618)
10	**% diff**	(3.8504)	(3.9711)	(3.8961)	(4.0222)	(3.9706)	(3.8760)	
	0.2	0.0837	0.0765	0.0708	0.0663	0.0625	0.0594	(29.0323)
	% diff	(7.9208)	(7.9422)	(8.0519)	(8.0444)	(8.0882)	(7.9070)	
	0	0.0230	0.0211	0.0195	0.0183	0.0172	0.0163	(29.1304)
	0.1	0.0221	0.0202	0.0187	0.0175	0.0166	0.0157	(28.9593)
20	**% diff**	(3.9130)	(4.2654)	(4.1026)	(4.3716)	(3.4884)	(3.6810)	
	0.2	0.0212	0.0194	0.0180	0.0168	0.0159	0.0150	(29.2453)
	% diff	(7.8261)	(8.0569)	(7.6923)	(8.1967)	(7.5581)	(7.9755)	

Table 4 Variation of frequency parameter with μ and a/h at (PM1, P = 10, *a/b* = 1)

Ti-6Al-4V/ZrO_2		**Nonlocal parameter (μ)**						
a/h	**ζ**	**0**	**1**	**2**	**3**	**4**	**5**	**% diff1**
	0	0.3047	0.2785	0.2580	0.2415	0.2278	0.2162	(29.0450)
	0.1	0.2843	0.2598	0.2407	0.2253	0.2125	0.2017	(29.0538)
5	**% diff**	(6.6951)	(6.7145)	(6.7054)	(6.7081)	(6.7164)	(6.7068)	
	0.2	0.2622	0.2396	0.2220	0.2078	0.1960	0.1860	(29.0618)
	% diff	(13.9481)	(13.9677)	(13.9535)	(13.9545)	(13.9596)	(13.9685)	

Table 4 continued

Ti-6Al-4V/ZrO_2		Nonlocal parameter (μ)						
a/h	ζ	**0**	**1**	**2**	**3**	**4**	**5**	**% diff1**
	0	0.0817	0.0747	0.0692	0.0648	0.0611	0.0580	(29.0086)
	0.1	0.0763	0.0697	0.0646	0.0605	0.0570	0.0541	(29.0957)
10	**% diff**	(6.6095)	(6.6934)	(6.6474)	(6.6358)	(6.7103)	(6.7241)	
	0.2	0.0704	0.0643	0.0596	0.0558	0.0526	0.0499	(29.1193)
	% diff	(13.8311)	(13.9224)	(13.8728)	(13.8889)	(13.9116)	(13.9655)	
	0	0.0207	0.0189	0.0175	0.0164	0.0155	0.0147	(28.9855)
	0.1	0.0193	0.0177	0.0164	0.0153	0.0145	0.0137	(29.0155)
20	**% diff**	(6.7633)	(6.3492)	(6.2857)	(6.7073)	(6.4516)	(6.8027)	
	0.2	0.0178	0.0163	0.0151	0.0141	0.0133	0.0127	(28.6517)
	% diff	(14.0097)	(13.7566)	(13.7143)	(14.0244)	(14.1935)	(13.6054)	

Table 5 Variation of frequency parameter with μ and a/h at (PM2, P = 10, *a/b* = 1)

Ti-6Al-4V/ZrO_2		Nonlocal parameter (μ)						
a/h	λ	**0**	**1**	**2**	**3**	**4**	**5**	**% diff1**
	0	0.3047	0.2785	0.2580	0.2415	0.2278	0.2162	(29.0450)
	0.1	0.2902	0.2652	0.2458	0.2300	0.2170	0.2059	(29.0489)
5	**% diff**	(4.7588)	(4.7756)	(4.7287)	(4.7619)	(4.7410)	(4.7641)	
	0.2	0.2753	0.2516	0.2331	0.2182	0.2058	0.1953	(29.0592)
	% diff	(9.6488)	(9.6589)	(9.6512)	(9.6480)	(9.6576)	(9.6670)	
	0	0.0817	0.0747	0.0692	0.0648	0.0611	0.0580	(29.0086)
	0.1	0.0780	0.0712	0.0660	0.0618	0.0583	0.0553	(29.1026)
10	**% diff**	(4.5288)	(4.6854)	(4.6243)	(4.6296)	(4.5827)	(4.6552)	
	0.2	0.0740	0.0677	0.0627	0.0587	0.0553	0.0525	(29.0541)
	% diff	(9.4247)	(9.3708)	(9.3931)	(9.4136)	(9.4926)	(9.4828)	
	0	0.0207	0.0189	0.0175	0.0164	0.0155	0.0147	(28.9855)
	0.1	0.0198	0.0181	0.0167	0.0157	0.0148	0.0140	(29.2929)
20	**% diff**	(4.3478)	(4.2328)	(4.5714)	(4.2683)	(4.5161)	(4.7619)	
	0.2	0.0188	0.0172	0.0159	0.0149	0.0140	0.0133	(29.2553)
	% diff	(9.1787)	(8.9947)	(9.1429)	(9.1463)	(9.6774)	(9.5238)	

(μ) increases from 0 to 1, the fundamental frequency decreases by approximately 10% whereas, on the further increment in the nonlocal parameter *(μ)* i.e., from 1 to 5, the influence of small-scale effects increases. Approximately 30% to 33% decrease in fundamental frequency has been found as the nonlocal parameter increases from 0 to 5 and around 7% to 10% reduction in frequency has been found as the porosity volume fraction increases from 0 to 0.2 in porosity model 1 and 2 respectively. As the side to thickness ratio *(a/h)* increases i.e., the nanoplate changes from thick to thin, the percentage reduction in fundamental frequency decreases from approximately 12% to 10% in thick plates to 5% to 7% in thin plates for varying porosity volume fraction. The percentage difference between non-porous FG nanoplates and porous nanoplate has also been reported with varying nonlocal parameter. The percentage difference has remained constant for varying nonlocal parameter and increased with increasing porosity volume fraction. Similar observations have been observed in all the cases of PM1 and PM2 models. % diff defines the percentage difference between non-porous and porous FG nanoplate and % diff1 defines the percentage difference between FG macro i.e., $\mu = 0$ and nanoplate i.e., $\mu = 5$.

It has been observed from the results that at certain operating parameters like nonlocal parameter *(μ)*, porosity volume fraction, side to thickness ratios *(a/h)*, etc., the value of fundamental frequency is less in the case of porosity model 1 in comparison with porosity model 2. This is due to the fact the first porosity model incorporates the even porosity in the plates whereas the second models cause the distribution of the uneven pores in the FG plates.

In Tables 4 and 5, both porosity model has been used for carrying out the vibrational analysis at volume fraction index of 10. It has been found that the fundamental

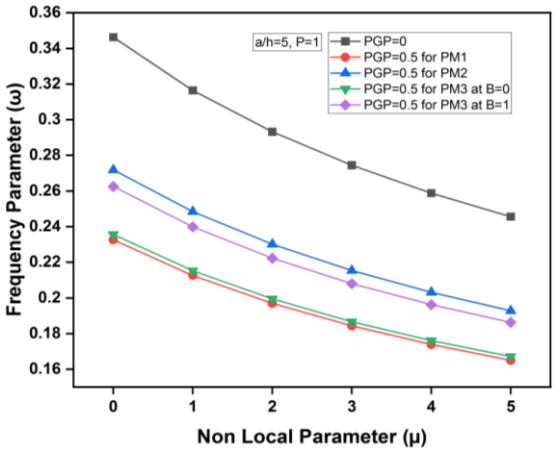

Fig. 6 VFP vs Nonlocal parameter at *a/h* = 5 and P = 1

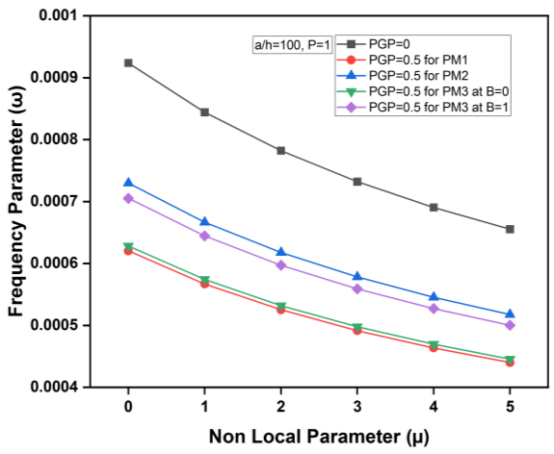

Fig. 8 VFP vs Nonlocal parameter at *a/h* = 100 and P = 1

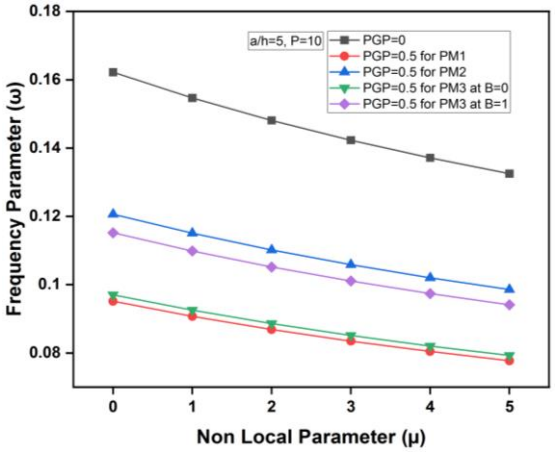

Fig. 7 VFP vs Nonlocal parameter at *a/h* = 5 and P = 10

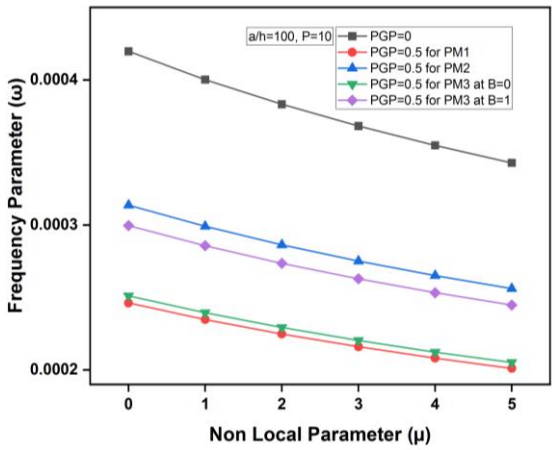

Fig. 9 VFP vs Nonlocal parameter at *a/h* = 100 and P = 10

frequency decreases with the increase in the porosity model parameter and nonlocal parameter *(μ)*. The fundamental frequency decreases by approximately 8% to 10% as the small-scale effects are incorporated and it decreases further as the nonlocal parameter or small-scale effects increases. Approximately 30% decrease in fundamental frequency has been found as the nonlocal parameter increased from 0 to 5 and 7% to 10% reduction in frequency has been found as the porosity volume fraction increases from 0 to 0.2 in porosity model 1 and 2 respectively. As the side to thickness ratio increases i.e., the nanoplate changes from thick to thin, the percentage reduction in fundamental frequency decreases from 12% to 10% in thick plates to 7% to 8% in thin plates for varying porosity parameters.

From Tables 2-5, it can be concluded that the fundamental frequency decreases as the side to thickness ratio *(a/h)* increases with increasing volume fraction index for simply supported square and porous FG nanoplates.

4.3.2 Comparative study of PM1, PM2, and PM3

In Figs. 6-9, the graphical comparison of porosity models 1, 2, and 3 have been done. A detailed comparison of the porosity model for different a/h ratios and volume fraction index has been reported. These graphs showed the variation of frequency for thick to thin plates in conjugation with nonlocal parameter and porosity governing parameter (PGP). The change in natural frequency with an increase in in the nonlocal parameter is quite significant for thick plates while for thin plates it is least significant. It has been found that the reduction in fundamental frequency is around 30% for thick plates while for moderately thin plates, it is around 25% to 30%. For thin plates, the values of the fundamental frequency are very less in comparison with thick plates. Results show that the newly developed porosity model (PM3) provides the results between PM1 and PM2 model which signifies that this new porosity model can predict the frequency values between even and uneven porosity models.

This change in fundamental frequency is observed at different volume fraction index (VFI) i.e., 1 and 10. With the increase in volume fraction index, the fundamental frequency decreases in both the porosity models. It signifies that as the ceramic content increases the fundamental frequency decreases.

4.3.3 Influence of newly developed generalized porosity model on FG nanoplate with varying μ, P, a/h and κ

The influence of various parameters like Nonlocal parameter, Volume fraction index, Side to thickness ratio,

Table 6 Variation of frequency parameter with μ and B at (PM3, a/h = 10, P = 1, κ = 0.2)

		Non-local parameter (μ)					
	B	0	1	2	3	4	5
	0	0.0806	0.0737	0.0683	0.0639	0.0603	0.0572
(1,1)	**0.5**	0.0821	0.0750	0.0695	0.0650	0.0613	0.0582
	1	0.0833	0.0761	0.0705	0.0660	0.0623	0.0591
	0	0.1970	0.1612	0.1398	0.1251	0.1143	0.1058
(1,2)	**0.5**	0.2005	0.1640	0.1422	0.1273	0.1162	0.1077
	1	0.2034	0.1665	0.1443	0.1292	0.1180	0.1092
	0	0.3086	0.2307	0.1922	0.1682	0.1513	0.1387
(2,2)	**0.5**	0.3139	0.2346	0.1954	0.1710	0.1539	0.1411
	1	0.3184	0.2380	0.1983	0.1735	0.1561	0.1431
	0	0.3806	0.2700	0.2207	0.1913	0.1711	0.1562
(1,3)	**0.5**	0.3870	0.2745	0.2244	0.1945	0.1740	0.1589
	1	0.3925	0.2785	0.2276	0.1972	0.1765	0.1611
	0	0.4854	0.3212	0.2570	0.2204	0.1960	0.1782
(2,3)	**0.5**	0.4933	0.3265	0.2612	0.2240	0.1992	0.1812
	1	0.5002	0.3311	0.2649	0.2272	0.2020	0.1837
	0	0.6523	0.3914	0.3057	0.2593	0.2291	0.2075
(3,3)	**0.5**	0.6627	0.3977	0.3106	0.2634	0.2327	0.2108
	1	0.6716	0.4031	0.3148	0.2670	0.2359	0.2136

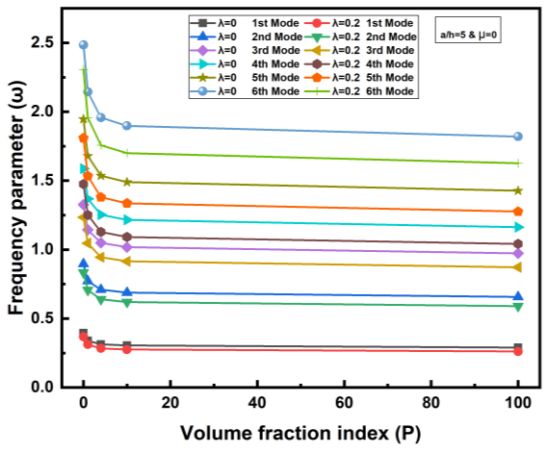

Fig. 10 Higher modes vs VFC at a/h = 5 and μ = 0

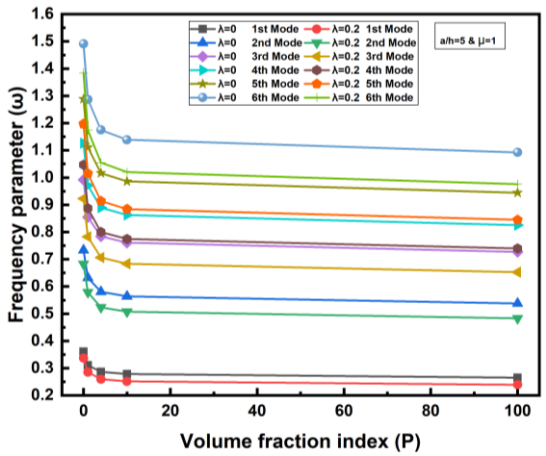

Fig. 11 Higher modes vs VFC at a/h = 5 and μ = 1

and porosity volume fraction have been observed on even and uneven porous FG nanoplate. The newly developed generalized porosity function has been employed to investigate the effects of various parameters on the natural frequency of the FG porous nanoplate.

In Table 6, the vibrational behavior of porous FG nanoplate using newly developed generalized porosity expression have been reported. It has been shown that the natural frequency of the porous FG nanoplate increases with changing the porous behavior from even to uneven. When the porous behavior changes from even to uneven, approximately 5% increase in the natural frequency has been found for initial modes and around 10%-12% increment for higher modes. Approximately 25% reduction has been found in the natural frequency for the first few modes and approximately 60% reduction in frequency has been found in higher modes of vibration as the small-scale effects are incorporated for varying nonlocal parameter from 1 to 5. It is also depicted in the table that as the modes of vibration increase the fundamental frequency of the porous nanoplate also increases.

4.3.4 Influence of porosity and nonlocal parameter on higher modes of vibration of FGM nanoplates

In Figs. 10-13, it has been shown that the variation of frequency at different modes of vibration with varying volume fraction coefficient (P). The reported results show the variation of frequency at higher modes of vibration with porosity model 1 for macro and nanoplates.

For thick and thin macro plate, the frequency parameter vs volume fraction index showed that the values of frequency increase with the increase in modes of vibration.

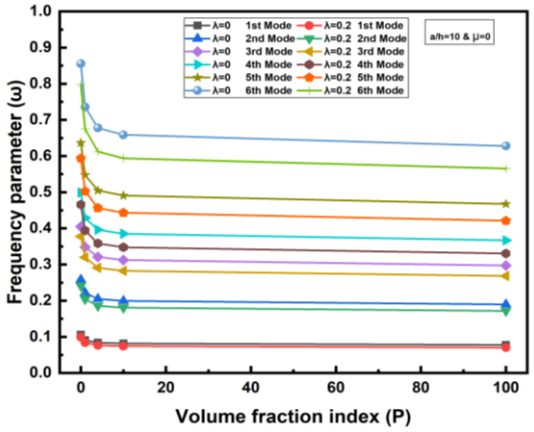

Fig. 12 Higher modes vs VFC at a/h = 10 and μ = 0

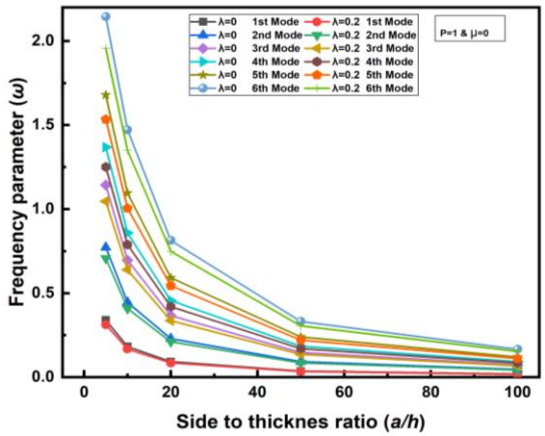

Fig. 14 Higher modes vs a/h at P = 1 and μ = 0

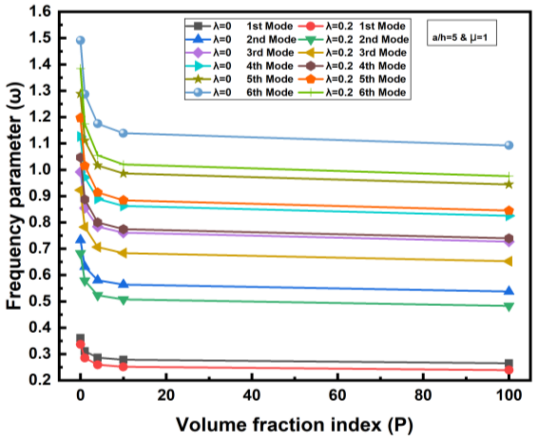

Fig. 13 Higher modes vs VFC at a/h = 10 and μ = 1

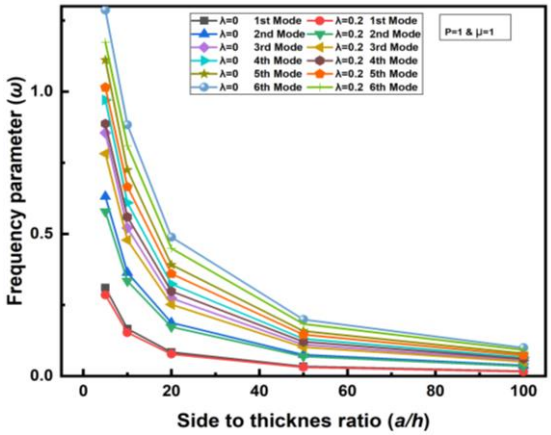

Fig. 15 Higher modes vs a/h at P = 1 and μ = 1

The result also shows that as the content of ceramic increases in the FG plate, the natural frequency decreases, and the frequency of the porous plate is always remaining lesser than the non-porous plate. The percentage difference between the frequency of porous and nonporous plate for particular mode increases at the higher modes i.e., (1, 1), (1, 2), (1, 3), (2, 2), and so on.

Similar behavior has also been observed in thick and thin nanoplate but in this case, a significant reduction in frequency has been observed in comparison with the macro plate. So, it has been observed that the incorporation of small-scale effects brings down the values of fundamental frequency even for higher modes of vibration.

In Figs. 14 and 15, the effect of varying side to thickness ratio (a/h) has also been observed for higher modes of vibration in both macro and nanoplate. It is observed that as the a/h ratio increases, the natural frequency of the plate decreases. The fundamental frequency of a porous plate remains lesser than the non-porous plate. The percentage difference between the frequency of porous and nonporous plate does not change significantly at the higher modes also.

4.4 Case II: Finite element solution

This section covers the comprehensive analysis of FEM based solution. As it is well known that the Navier solution is only applicable to simply supported boundary conditions therefore to analyze various other boundary conditions FEM solution is used. In this section, various unconventional i.e., partially supported boundary conditions have been incorporated in FG nanoplate and studied comprehensively with varying nonlocal parameters and porosity governing parameter of porosity model i.e., PM3.

4.4.1 Parametric studies using partially supported boundary conditions

In this section, partially supported boundary conditions have been with various clamping ratios as described in Fig. 16. A square plate of 16X16 mesh has been considered for analysis with different clamping ratios (CR) i.e., Length of clamped part /total length of the plate (4a). It is well known that the plate has always been considered as the most important part of structures. Acquiring various discontinuities along the boundaries has always been a cause of concern. So, to provide more realistic results, the partially supported boundary conditions have also been analyzed in comparison with conventional boundary conditions.

Figs. 17-28 report the vibrational behavior of the square plate for different cases of partially supported FG porous nanoplate with varying porosity governing parameters and Nonlocal parameter. In all the unconventional boundary conditions, the comparative results have been shown as the volume fraction index changes from 0 to 1. It has been observed in the reported results that the fundamental

frequency of the FG porous plate gets reduced as the volume fraction index increases.

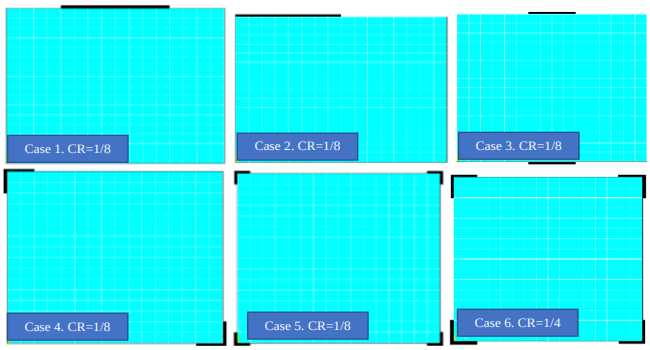

Fig. 16 Partially supported (16X16) meshed square plates

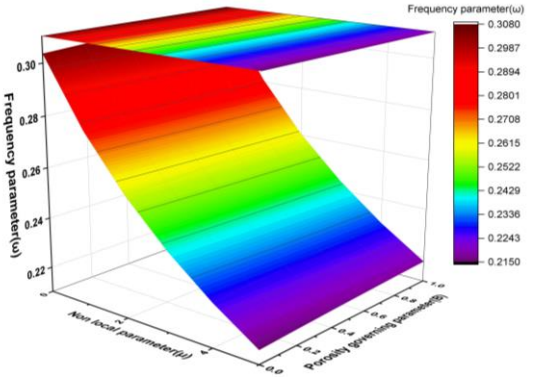

Fig. 17 VFP vs μ and B, Case 1 at P = 0 and a/h = 10

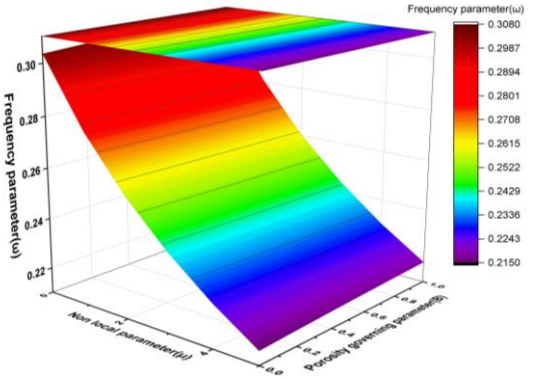

Fig. 18 VFP vs μ and B, Case 1 at P = 1 and a/h = 10

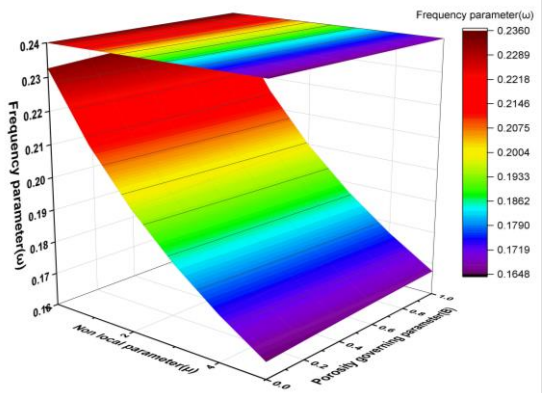

Fig. 19 VFP vs μ and B, Case 2 at P = 0 and a/h = 10

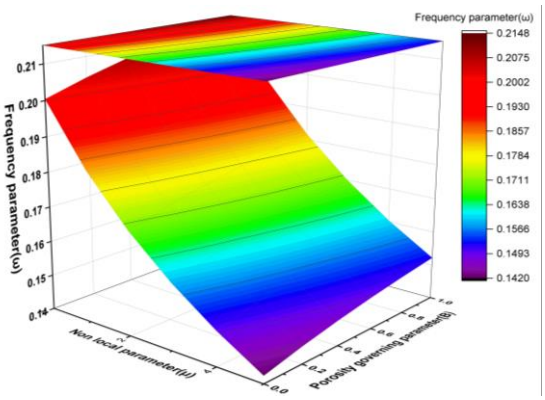

Fig. 20 VFP vs μ and B, Case 2 at P = 1 and a/h = 10

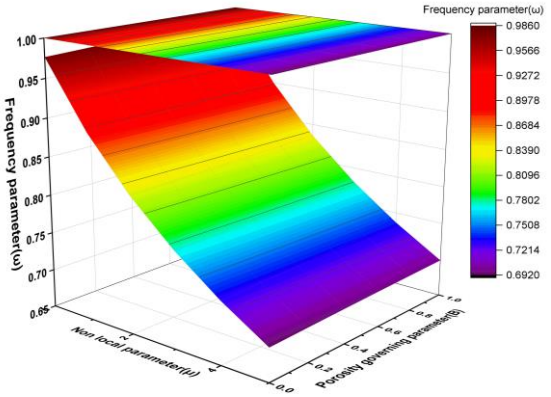

Fig. 21 VFP vs μ and B, Case 3 at P = 0 and a/h = 10

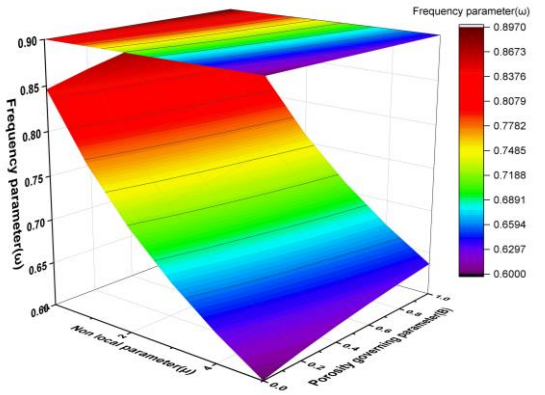

Fig. 22 VFP vs μ and B, Case 3 at P = 1 and a/h = 1

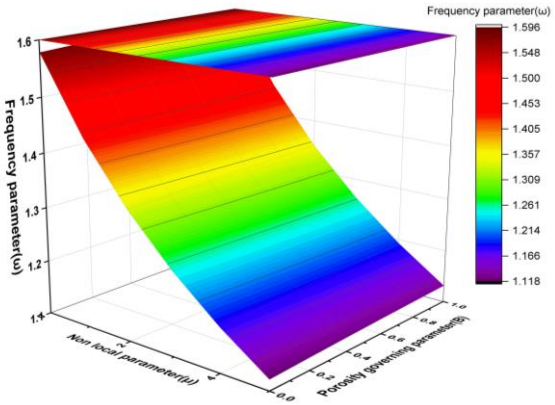

Fig. 23 VFP vs μ and B, Case 4 at P = 0 and a/h = 10

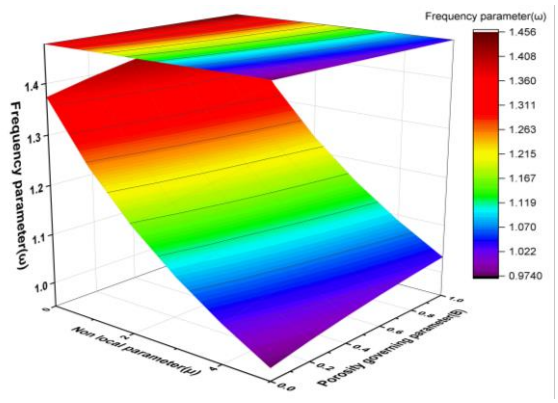

Fig. 24 VFP vs μ and B, Case 4 at P = 1 and *a/h* = 10

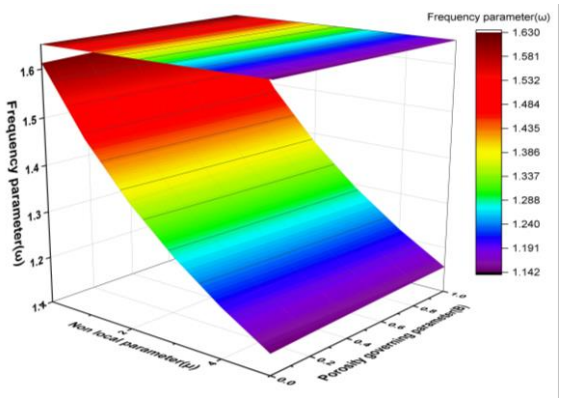

Fig. 25 VFP vs μ and B, Case 5 at P = 0 and *a/h* = 10

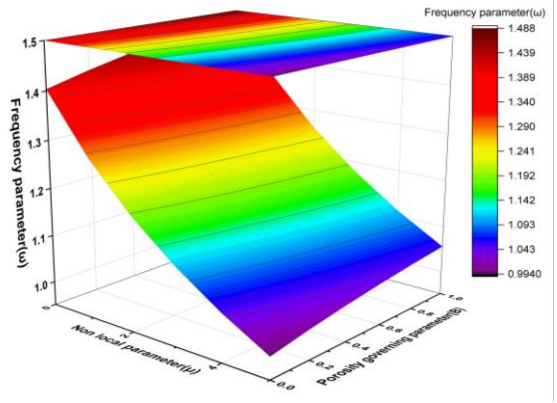

Fig. 26 VFP vs μ and B, Case 5 at P = 1 and *a/h* = 10

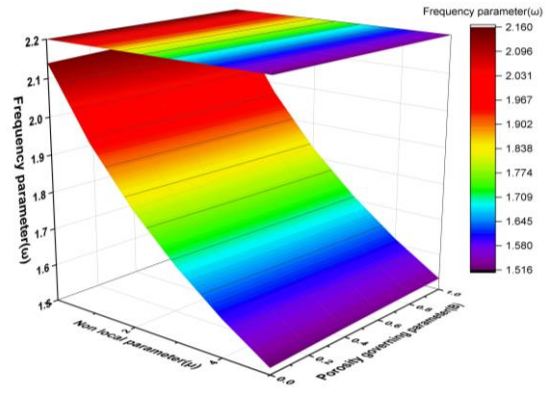

Fig. 27 VFP vs μ and B, Case 6 at P = 0 and *a/h* = 10

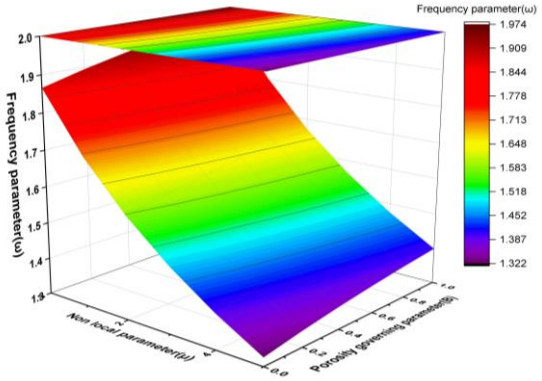

Fig. 27 VFP vs μ and B, Case 6 at P = 1 and *a/h* = 10

5. Conclusions

In this present paper, the detailed vibrational analysis of FG porous nanoplate has been carried out using exact i.e. Navier method and approximate i.e. Finite element method. The non-polynomial based refined trigonometric higher-order shear deformation theory has been developed in conjunction with nonlocal theory to capture the small-scale effects. In the analysis, it has been found that the incorporation of the nonlocal parameter and porosity volume fraction has a significant effect on nanoplate.

The influence of various parameters like side to thickness ratio (*a/h*), aspect ratios, volume fraction index (*P*), Nonlocal parameter (μ) with existing and newly developed generalized porosity models have been observed and reported. Various observations from the above analysis are as follows.

- The reduction in fundamental frequency has been observed with the increase in side to thickness ratio and volume fraction index. Around 12% reduction in frequency values have been observed in thick plates and around 7% in thin plates as the plate changes from nonporous to porous plate.
- With the incorporation of small-scale effects, the percentage reduction in fundamental frequency is more pronounced. Around 30% reduction in frequency values has been observed as the nonlocal parameter incorporated.
- The behavior of all three porosity models has also been reported with varying nonlocal parameter for thick and thin nanoplate at certain volume fraction index.
- The newly developed generalized porosity model has been analyzed for varying nonlocal parameters, volume fraction index, etc. It has been found that the values of natural frequency increase for uneven porous behavior and decrease the values of nonlocal parameter, volume fraction index, and side to thickness ratio increases.
- Higher modes of vibration have also been reported in the present study. It has been shown that the natural frequency of the nanoplate is increased with the increases in modes of vibration. At higher modes of vibration, the percentage is a difference in porosity models is quite high in comparison at lower modes.
- Effects of varying non-local parameters, Volume fraction index and porosity volume fractions on frequency

parameters have been analyzed using the finite element method with conventional and unconventional boundary conditions.

So, in the present paper, a detailed account of FG porous nanoplate has been presented. The results produced in this study will provide a holistic view to the Design engineer.

References

Arefi, M. and Rabczuk, T. (2019), "A nonlocal higher order shear deformation theory for electro-elastic analysis of a piezoelectric doubly curved nano shell", *Compos. Part B Eng.*, **168**, 496-510. https://doi.org/10.1016/j.compositesb.2019.03.065.

Barretta, R. and de Sciarra, F.M. (2018), "Constitutive boundary conditions for nonlocal strain gradient elastic nano-beams", *Int. J. Eng. Sci.*, **130**, 187-198. https://doi.org/10.1016/j.ijengsci.2018.05.009.

Barretta, R. and de Sciarra, F.M. (2019), "Variational nonlocal gradient elasticity for nano-beams", *Int. J. Eng. Sci.*, **143**, 73-91. https://doi.org/10.1016/j.ijengsci.2019.06.016.

Barretta, R., Faghidian, S.A. and De Sciarra, F.M. (2019a), "Stress-driven nonlocal integral elasticity for axisymmetric nano-plates", *Int. J. Eng. Sci.*, **136**, 38-52. https://doi.org/10.1016/j.ijengsci.2019.01.003.

Barretta, R., Caporale, A., Faghidian, S.A., Luciano, R., de Sciarra, F.M. and Medaglia, C.M. (2019b), "A stress-driven local-nonlocal mixture model for Timoshenko nano-beams", *Compos. Part B Eng.*, **164**, 590-598.https://doi.org/10.1016/j.compositesb.2019.01.012.

Barretta, R., Fabbrocino, F., Luciano, R., De Sciarra, F.M. and Ruta, G. (2020), "Buckling loads of nano-beams in stress-driven nonlocal elasticity", *Mech. Adv. Mater. Struct.*, **27**(11), 869-875. https://doi.org/10.1080/15376494.2018.1501523.

Batou, B., Nebab, M., Bennai, R., Atmane, H.A., Tounsi, A. and Bouremana, M. (2019), "Wave dispersion properties in imperfect sigmoid plates using various HSDTs", *Steel Compos. Struct.*, **33**(5), 699-716. http://doi.org/10.12989/scs.2019.33.5.699.

Belkorissat, I., Houari, M.S.A., Tounsi, A., Bedia, E.A. and Mahmoud, S.R. (2015), "On vibration properties of functionally graded nano-plate using a new nonlocal refined four variable model", *Steel Compos. Struct.*, **18**(4), 1063-1081. https://doi.org/10.12989/scs.2015.18.4.1063.

Ebrahimi, F. and Jafari, A. (2017), "Investigating vibration behavior of smart imperfect functionally graded beam subjected to magnetic-electric fields based on refined shear deformation theory", *Adv. Nano Res.*, **5**(4), 281. https://doi.org/10.12989/anr.2017.5.4.281.

Ebrahimi, F., Karimiasl, M. and Mahesh, V. (2019a), "Vibration analysis of magneto-flexo-electrically actuated porous rotary nanobeams considering thermal effects via nonlocal strain gradient elasticity theory", *Adv. Nano Res.*, **7**(4), 223-231. http://doi.org/10.12989/anr.2019.7.4.223.

Ebrahimi, F., Hosseini, S.H.S. and Bayrami, S.S. (2019b), "Nonlinear forced vibration of pre-stressed graphene sheets subjected to a mechanical shock: An analytical study". *Thin Wall. Struct.*, **141**, 293-307. https://doi.org/10.1016/j.tws.2019.04.038.

Eringen, A.C. (1983), "On differential equations of nonlocal elasticity and solutions of screw dislocation and surface waves", *J. Appl. Phys.*, **54**(9), 4703-4710. https://doi.org/10.1063/1.332803.

Eringen, A.C. and Edelen, D.G.B. (1972), "On nonlocal elasticity", *Int. J. Eng. Sci.*, **10**(3), 233-248. https://doi.org/10.1016/0020-7225(72)90039-0.

Fenjan, R.M., Ahmed, R.A., Faleh, N.M. and Fatima, F.M. (2020a), "Numerical investigation on scale-dependent vibrations of porous foam plates under dynamic loads", *Struct. Monitor. Maintenance*, **7**(2), 85-107.http://dx.doi.org/10.12989/smm.2020.7.2.085.

Fenjan, R.M., Ahmed, R.A., Faleh, N.M. and Hani, F.M. (2020b), "Dynamic response of size-dependent porous functionally graded beams under thermal and moving load using a numerical approach", *Struct. Monitor. Maintenance*, **7**(2), 69-84. http://doi.org/10.12989/smm.2020.7.2.069.

Ghabussi, A., Habibi, M., NoormohammadiArani, O., Shavalipour, A., Moayedi, H. and Safarpour, H. (2021), "Frequency characteristics of a viscoelastic graphene nanoplatelet–reinforced composite circular microplate", *J. Vib. Control*, **27**(1-2), 101-118. https://doi.org/10.1177%2F1077546320923930.

Gholami, R. and Ansari, R. (2018), "Imperfection sensitivity of post-buckling behavior and vibration response in pre-and post-buckled regions of nanoscale plates considering surface effects", *Int. J. Appl. Mech.*, **10**(3), 1850027. https://doi.org/10.1142/S1758825118500278.

Gupta, A. and Talha, M. (2017), "Nonlinear flexural and vibration response of geometrically imperfect gradient plates using hyperbolic higher-order shear and normal deformation theory", *Compos. Part B Eng.*, **123**, 241-261. https://doi.org/10.1016/j.compositesb.2017.05.010.

Gupta, A. and Talha, M. (2018a), "Influence of micro-structural defects on post-buckling and large-amplitude vibration of geometrically imperfect gradient plate", *Nonlinear Dynam.*, **94**(1), 39-56. https://doi.org/10.1007/s11071-018-4344-5.

Gupta, A. and Talha, M. (2018b), "Influence of porosity on the flexural and free vibration responses of functionally graded plates in thermal environment", *Int. J. Struct. Stabil. Dynam.*, **18**(1), 1850013. https://doi.org/10.1142/S021945541850013X.

Jha, D.K., Kant, T. and Singh, R.K. (2013), "Free vibration response of functionally graded thick plates with shear and normal deformations effects", *Compos. Struct.*, **96**, 799-823. http://doi.org/10.1016/j.compstruct.2012.09.034.

Karami, B. and Janghorban, M. (2019), "On the dynamics of porous nanotubes with variable material properties and variable thickness", *Int. J. Eng. Sci.*, **136**, 53-66. https://doi.org/10.1016/j.ijengsci.2019.01.002.

Karami, B., Shahsavari, D. and Janghorban, M. (2019), "On the dynamics of porous doubly-curved nanoshells", *Int. J. Eng. Sci.*, **143**, 39-55. https://doi.org/10.1016/j.ijengsci.2019.06.014.

Koizumi, M.F.G.M. (1997), "FGM activities in Japan", *Compos. Part B Eng.*, **28**(1-2), 1-4. https://doi.org/10.1016/S1359-8368(96)00016-9.

Liang, Y.C., Dou, J.H. and Bai, Q.S. (2007), "Molecular dynamic simulation study of AFM single-wall carbon nanotube tip-surface interactions", *Key Eng. Mater.*, **339**, 206-210. https://doi.org/10.4028/www.scientific.net/KEM.339.206.

Mantari, J.L. and Monge, J.C. (2016), "Buckling, free vibration and bending analysis of functionally graded sandwich plates based on an optimized hyperbolic unified formulation", *Int. J. Mech. Sci.*, **119**, 170-186. https://doi.org/10.1016/j.ijmecsci.2016.10.015.

Mehar, K., Mahapatra, T.R., Panda, S.K., Katariya, P.V. and Tompe, U.K. (2018), "Finite-element solution to nonlocal elasticity and scale effect on frequency behavior of shear deformable nanoplate structure", *J. Eng. Mech.*, **144**(9), 04018094. https://orcid.org/0000-0001-8841-7449.

Patil, S.A., Shinde, D.V., Patil, D.V., Tehare, K.K., Jadhav, V.V., Lee, J.K., Mane, R.S., Shrestha, N.K. and Han, S.H. (2014), "A simple, room temperature, solid-state synthesis route for metal oxide nanostructures", *J. Mater. Chem. A*, **2**(33), 13519-13526. https://doi.org/10.1039/C4TA02267J.

Ramirez, D., Cuba, L., Mantari, J.L. and Arciniega, R.A. (2019),

"Bending and free vibration analysis of functionally graded plates via optimized non-polynomial higher order theories", *J. Appl. Computat. Mech.*, **5**(2), 281-298. https://doi.org/10.22055/JACM.2018.25177.1237.

Romano, G., Barretta, R., Diaco, M. and de Sciarra, F.M. (2017), "Constitutive boundary conditions and paradoxes in nonlocal elastic nanobeams", *Int. J. Mech. Sci.*, **121**, 151-156. https://doi.org/10.1016/j.ijmecsci.2016.10.036.

Sarangan, S. and Singh, B.N. (2016), "Higher-order closed-form solution for the analysis of laminated composite and sandwich plates based on new shear deformation theories", *Compos. Struct.*, **138**, 391-403. https://doi.org/10.1016/j.compstruct.2015.11.049.

Sedighi, H.M., Daneshmand, F. and Abadyan, M. (2015), "Dynamic instability analysis of electrostatic functionally graded doubly-clamped nano-actuators", *Compos. Struct.*, **124**, 55-64. http://doi.org/10.1016/j.compstruct.2015.01.004.

Sedighi, H.M., Daneshmand, F. and Abadyan, M. (2016), "Modeling the effects of material properties on the pull-in instability of nonlocal functionally graded nano-actuators", *ZAMM J. Appl. Math. Mech.* **96**(3), 385-400. https://doi.org/10.1002/zamm.201400160.

Shariati, A., Mohammad-Sedighi, H., Żur, K.K., Habibi, M. and Safa, M. (2020), "On the vibrations and stability of moving viscoelastic axially functionally graded nanobeams", *Materials*, **13**(7), 1707. https://doi.org/10.3390/ma13071707.

Sobhy, M. and Radwan, A.F. (2017), "A new quasi 3D nonlocal plate theory for vibration and buckling of FGM nanoplates", *Int. J. Appl. Mech.*, **9**(1), 1750008. https://doi.org/10.1142/S1758825117500089.

Sun, C.T. and Zhang, H. (2003), "Size-dependent elastic moduli of platelike nanomaterials", *J. Appl. Phys.*, **93**(2), 1212-1218. https://doi.org/10.1063/1.1530365.

Thai, H.T. and Choi, D.H. (2013), "Efficient higher-order shear deformation theories for bending and free vibration analyses of functionally graded plates", *Arch. Appl. Mech.*, **83**(12), 1755-1771. http://doi.org/10.1007/s00419-013-0776-z.

Yang, X., Liu, H. and Ma, J. (2020), "Thermo-mechanical vibration of FG curved nanobeam containing porosities and reinforced by graphene platelets", *Microsyst. Technol.*, **26**(8), 2535-2551. https://doi.org/10.1007/s00542-020-04794-w.

Zhu, R., Pan, E. and Roy, A.K. (2007), "Molecular dynamics study of the stress–strain behavior of carbon-nanotube reinforced Epon 862 composites", *Mater. Sci. Eng. A*, **447**(1-2), 51-57. https://doi.org/10.1016/j.msea.2006.10.054.

CC